Journal of Power Sources 255 (2014) 170–178

Contents lists available at ScienceDirect

Journal of Power Sources

journal homepage: www.elsevier.com/locate/jpowsour

A facile approach to fabricate flexible all-solid-state supercapacitors based on $MnFe_2O_4$/graphene hybrids

Weihua Cai, Ting Lai, Wanlin Dai, Jianshan Ye*

College of Chemistry and Chemical Engineering, South China University of Technology, Guangzhou 510641, PR China

HIGHLIGHTS

- A facile approach is proposed to fabricate all-solid-state supercapacitors.
- $MnFe_2O_4$/graphene hybrids achieve a capacitance of 300 F g^{-1} at 0.3 A g^{-1}.
- Our devices show excellent electrochemical performance and cycling stability.

GRAPHICAL ABSTRACT

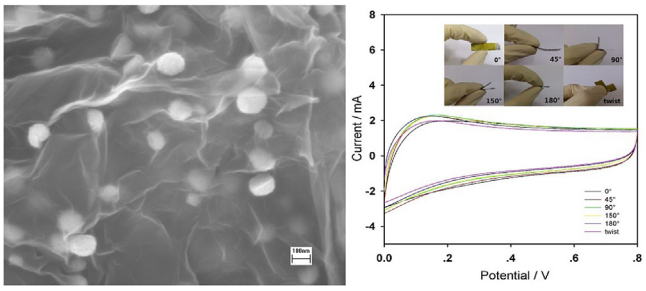

ARTICLE INFO

Article history:
Received 26 October 2013
Received in revised form
4 January 2014
Accepted 6 January 2014
Available online 14 January 2014

Keywords:
Flexible electrochemical capacitors
Supercapacitors
Manganese ferrite
Graphene
All-solid-state devices

ABSTRACT

A critical challenge for the construction of flexible electrochemical capacitors is the preparation of flexible electrodes with large specific capacitance and robust mechanical strength. Here, we demonstrate a facile approach to make high performance and flexible electrodes by dropping $MnFe_2O_4$/graphene hybrid inks onto flexible graphite sheets (as current collectors and substrates) and drying under an infrared lamp. $MnFe_2O_4$/graphene hybrid inks are synthesized by immobilizing the $MnFe_2O_4$ microspheres on the graphene nanosheets via a simple solvothermal route. Electrochemical studies show that $MnFe_2O_4$/graphene exhibits a high capacitance of 300 F g^{-1} at a current density of 0.3 A g^{-1}. In addition, the excellent electrochemical performance of a supercapacitor consisting of a sandwich structure of two pieces of $MnFe_2O_4$/graphene hybrids modified electrodes separated by polyvinyl alcohol (PVA)-H_2SO_4 gel electrolyte is further explored. Our studies reveal that the flexible supercapacitor device with 227 μm thickness can achieve a maximum specific capacitance of 120 F g^{-1} at a current density of 0.1 A g^{-1} and excellent cycle performance retaining 105% capacitance after 5000 cycles. This research may offer a method for the fabrication of lightweight, stable, flexible and high performance energy storage devices.

1. Introduction

Flexible electrochemical capacitors (also called supercapacitors) draw attentions because of their potential applications in portable and flexible electronics, such as electronic papers, roll-up displays and wearable devices [1–3]. Based on the mechanism of the charge storage, electrochemical capacitors could be divided into electric double layer capacitors (EDLCs) and pseudocapacitors. The pseudocapacitors using redox active material such as ruthenium oxide (RuO_2) [4–6], copper(II) oxide (CuO) [7–9], manganese dioxide (MnO_2) [10–12], cobaltosic oxide (Co_3O_4) [13–15] and vanadium pentoxide (V_2O_5) [16–19] usually exhibit larger specific capacitance than conventional EDLCs. For instance, the low-cost active material MnO_2 based electrode can achieves a high specific capacitance up to 678 F g^{-1} [20]. However, MnO_2 based pseudocapacitors suffer large capacitance loss after several thousands' charge/discharge cycling, i.e. about 20% capacitance loss as reports [10,20]. This

* Corresponding author. Tel.: +86 20 87113241; fax: +86 20 87112901.
E-mail address: jsye@scut.edu.cn (J. Ye).

0378-7753/$ – see front matter © 2014 Elsevier B.V. All rights reserved.
http://dx.doi.org/10.1016/j.jpowsour.2014.01.027

decrease of the capacitance probably resulted from the mechanical expansion of MnO_2 during the charge/discharge cycling. Interestingly, manganese ferrite ($MnFe_2O_4$) has been found to exhibit unusually large capacitances among ferrites including MFe_2O_4 where M = Mn, Fe, Co, or Ni [21]. Though with far superior cycling stability to amorphous MnO_2 electrode, the reported specific capacitance of $MnFe_2O_4$/carbon black of *ca.* 56.2 F g^{-1} is so limited [22].

Recently, graphene has attracted much interest as additive or supporter for metal oxide due to its outstanding conductivity and ultrahigh specific area. Graphene nanosheets-Fe_3O_4 [23], graphene/MnO_2 composite networks [10] and vanadium oxide nanowire-graphene nanocomposite [16] with various sizes and shapes have been synthesized by using different methods. A latest research reported a composite of MnO_2 grown on graphene, which showed high specific capacitances of 267 F g^{-1} as planar supercapacitor electrode [11]. Graphene, with two-dimensional structure, provides large surfaces to well anchor metal oxide particles and supports highways for the transport of electrons. Additionally, the metal oxides deposited on the surface of graphene keep graphene sheets well separated from strong Vander Waals interactions [16].

Our work was originally motivated to investigate the capacitive behaviors of $MnFe_2O_4$ microspheres grown on graphene nanosheets. In this study, solvothermal method was employed to fabricate $MnFe_2O_4$/graphene hybrids. Here, we propose a facile approach, for the first time, to manufacture high performance and flexible electrodes by dropping $MnFe_2O_4$/graphene hybrid inks onto flexible graphite sheets and dried under an infrared lamp in ambient condition. Furthermore, an all-solid-state flexible device with excellent electrochemical performance of maximum specific capacitance of 120 F g^{-1} at a current density of 0.1 A g^{-1} and with outstanding cycling performance was assembled. The stable and flexible supercapacitors in series could be used to successfully power a liquid crystal display (LCD).

2. Experimental

2.1. Chemicals and materials

Natural flake graphite was obtained from Sigma–Aldrich. Flexible graphite sheets (GTS) were purchased from Beichuan Co. Ltd (China). $FeCl_3 \cdot 6H_2O$, $MnCl_2 \cdot 4H_2O$ polyethylene glycol (PEG, molecules mass about 600) and polyvinyl alcohol AH-26 (PVA) were bought from Sinopharm Chemical Reagent Co. Ltd (China). All other chemicals were from local chemical agent, and de-ionized (DI) water (>18.4 MΩ cm^{-1}) was used throughout.

2.2. Preparation of graphite oxide

Graphite oxide (GO) was synthesized from natural flake graphite by a modified Hummers method [24]. In a typical procedure, $K_2S_2O_8$ (10 g) and P_2O_5 (10 g) and graphite powder (12 g) were put into concentrated H_2SO_4 (50 mL) at 80 °C. The above solution was stirred at 80 °C for 4.5 h. After cooling to room temperature, the solution was diluted with about 2 L of DI water and allowed to stand overnight. The supernatant was decanted, and the sediment was washed several times with DI water and centrifuged. The pretreated graphite was dried in air at 100 °C for 12 h. This pretreated graphite powder (2 g) was put into concentrated H_2SO_4 (50 mL) in an ice bath. $KMnO_4$ (7 g) was added gradually with stirring, and the temperature of the solution was kept below 10 °C. After the mixture was stirred at 35 °C for 2 h, 96 mL DI water was added. The solution was then stirred for another 30 min, and the reaction was then terminated by adding 300 mL of DI water and 5 mL of 30% H_2O_2 solution. The mixture was further washed with 500 mL of 10% HCl solution. The as-obtained GO was re-dispersed in DI water and then was dialyzed for one week to remove residual salts and acids.

2.3. Preparation of active materials

The preparation of $MnFe_2O_4$/graphene hybrids is based on a facile one-pot solvothermal method [25]. Typically, 60.0 mg of GO, 32.4 mg (0.12 mmol) of $FeCl_3 \cdot 6H_2O$, and 11.8 mg (0.06 mmol) of $MnCl_2 \cdot 4H_2O$ were dispersed in 40 mL of ethylene glycol with ultrasonication for 2 h. Subsequently, 2.16 g NaAc and 1.0 g polyethylene glycol were added, followed by stirring for 30 min. The mixture was then transferred to a Teflon-lined stainless steel autoclave and heated at 200 °C for 10 h. The obtained black product was washed with DI water and ethanol several times and was dried at 60 °C in a vacuum oven. For comparison, $MnFe_2O_4$/graphene hybrids with different initial metal ion concentrations (97.2 mg $FeCl_3 \cdot 6H_2O$ and 35.4 mg $MnCl_2 \cdot 4H_2O$ for the sample 3-$MnFe_2O_4$/graphene; 162.0 mg $FeCl_3 \cdot 6H_2O$ and 59.0 mg $MnCl_2 \cdot 4H_2O$ for the sample 5-$MnFe_2O_4$/graphene; 324.0 mg $FeCl_3 \cdot 6H_2O$ and 118.0 mg $MnCl_2 \cdot 4H_2O$ for the sample 10-$MnFe_2O_4$/graphene) were also prepared. Besides, the solvothermal graphene (s-graphene) and $MnFe_2O_4$ microspheres were prepared as reported [26,27].

2.4. Flexible electrode preparation

First, to prepare $MnFe_2O_4$/graphene hybrid inks, 2.0 mg $MnFe_2O_4$/graphene hybrids were added into 1 mL ethanol and ultra-sonicated for 3 min to produce a 2.0 mg mL^{-1} $MnFe_2O_4$/graphene hybrid inks. The $MnFe_2O_4$/graphene hybrids modified electrode can be easily prepared by dropping 100 μL of $MnFe_2O_4$/graphene hybrids inks (2.0 mg mL^{-1}) onto GTS and further dried under an infrared lamp in the ambient condition. Before the above procedure, GTS was cut into 1 cm × 2 cm electrode and was wrapped with Kapton tape to make sure that one end of the electrode possesses an area of 1 cm × 1 cm and the other end of the electrode would be clamped by alligator clips in the later experiments. Besides, the preparation of s-graphene inks and $MnFe_2O_4$ microspheres inks was based on the similar procedure for comparison in the following measurement.

2.5. Fabrication of all-solid-state devices

PVA-H_2SO_4 gel was used as a solid electrolyte. PVA-H_2SO_4 electrolyte was simply made as follows: 1.0 g H_2SO_4 was mixed with 10 mL DI water and then 1.0 g PVA powder was added. The whole mixture was heated to 90 °C under vigorously stirring until the solution became clear. The solid-state device was fabricated with two pieces of modified electrodes. An all-solid-state device was assembled by pouring the polymer gelled electrolyte (about 100 μL electrolyte 1 cm^{-2} of the electrode) slowly onto the modified electrodes. This assembly was left under ambient conditions for 5 h to ensure that the electrolyte completely wets the electrode and to allow for evaporation of any excess water. Two electrodes were then assembled face-to-face and left overnight until the electrolyte solidified.

2.6. Characterization

Scanning electron microscope (SEM) and Field emission scanning electron microscopy (FESEM) images were recorded on Hitachi S-3700 with an accelerating voltage of 10.0 kV or 20.0 kV and LEO 1530 VP with an accelerating voltage of 5.0 kV, respectively. X-ray diffraction (XRD) patterns were collected from a Bruker AXS D8-Advanced diffractometer with Cu Kα radiation (λ = 1.5418 Å). All electrochemical measurements were performed on a CHI660E

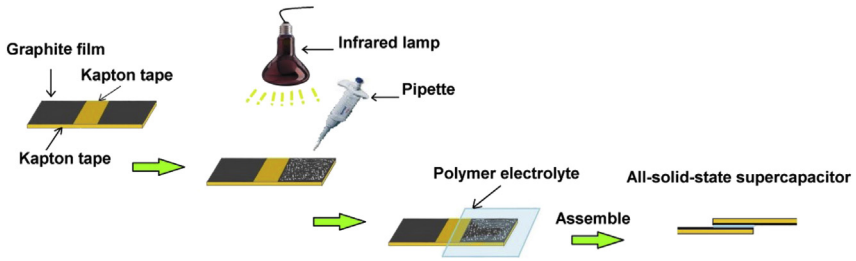

Fig. 1. Schematic diagram of the fabrication process of flexible all-solid-state supercapacitors.

electrochemical workstation (Chenhua, China). A three-electrode system was carried out with a flexible electrode as a working electrode with effective area of 1 cm × 1 cm, an Ag|AgCl (3.0 M KCl) reference electrode and a platinum wire counter electrode. Electrical measurements (*I*–*V* curves) were carried out on a CHI660E electrochemical workstation (using a two-electrode setup) by measuring the current produced at different gate voltages (from −0.5 to 0.5) with a potentiostatic technique. Conductivity values were calculated from the slopes of the *I*–*V* curves and the thickness of each film which was measured using cross-sectional SEM.

3. Results and discussion

Fig. 1 shows the processing steps to fabricate $MnFe_2O_4$/graphene hybrids based all-solid-state supercapacitors. One modified electrode used in the supercapacitor possesses the active materials of 0.2 mg cm^{-2}. After the supercapacitors were assembled, they were pressed under a pressure of about 1 MPa for 10 min, which made the polymer gel electrolyte into one thin separating layer. The resulting device was flexible and robust.

The morphologies of the as-prepared s-graphene, $MnFe_2O_4$ microspheres, $MnFe_2O_4$/graphene hybrids were characterized by SEM and FESEM techniques, as shown in Fig. 2. In the case of s-graphene (Fig. 2A), aggregates of crumpled sheets of graphene could be observed, similar to what has been reported [26]. Fig. 2B clearly demonstrates that monodispersed $MnFe_2O_4$ microspheres could be well distributed on GTS after the electrode was modified with $MnFe_2O_4$ inks and dried under an infrared lamp. As compared to severely agglomerated s-graphene, thin graphene sheets with $MnFe_2O_4$ microspheres could be seen from the FESEM image (Fig. 2C). A high resolution FESEM image (Fig. 2D) indicates that flake-like graphene nanosheets are coated with $MnFe_2O_4$ microspheres. The characterization above indicates the presence of $MnFe_2O_4$ microspheres can prevent the graphene sheets from severe agglomeration. A cross-sectional SEM image (Fig. 2E) of the

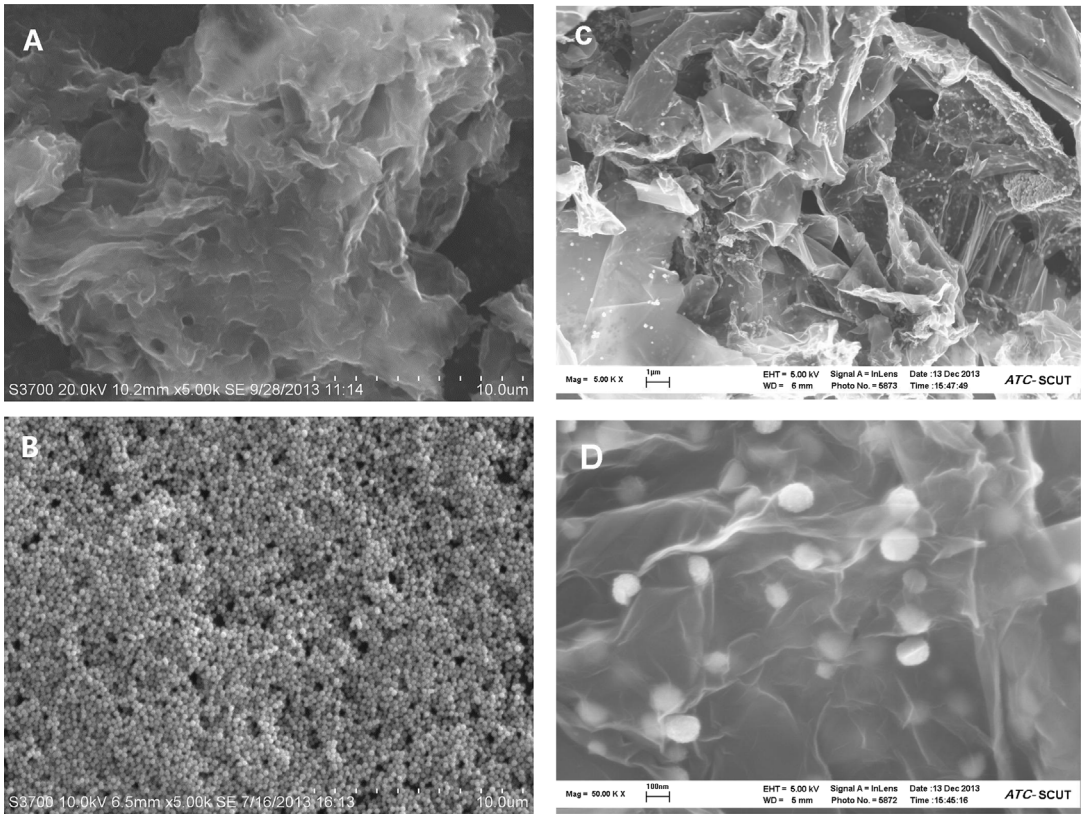

Fig. 2. SEM images of (A) s-graphene, (B) $MnFe_2O_4$ microspheres; (C) FESEM images of $MnFe_2O_4$/graphene hybrids; (D) high resolution FESEM image of $MnFe_2O_4$/graphene hybrids; (E) a cross-sectional SEM image of the flexible device based on $MnFe_2O_4$/graphene hybrids with mass loading of 0.4 mg; (F) EDS mapping analysis of $MnFe_2O_4$/graphene.

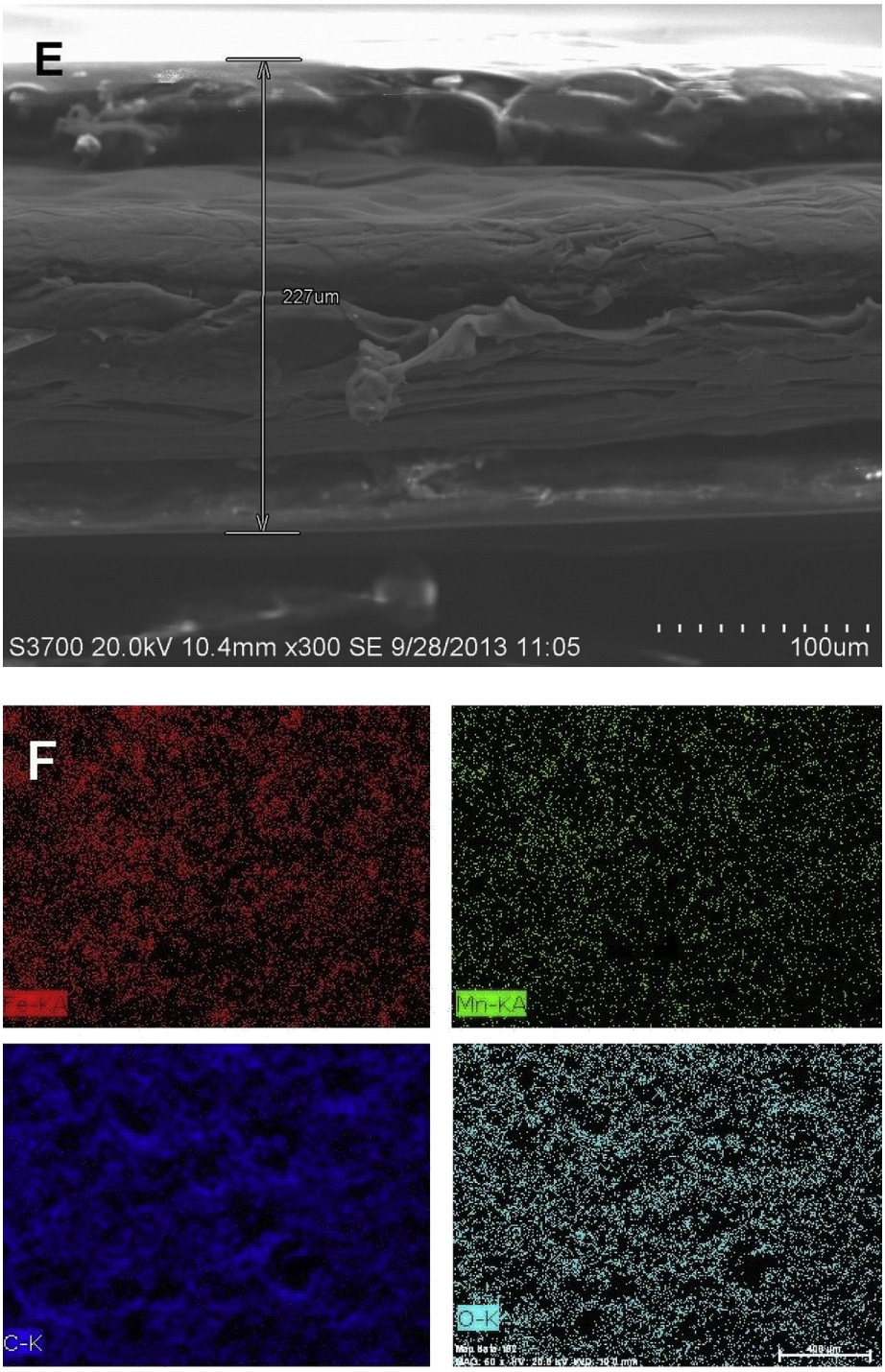

Fig. 2. (*continued*).

flexible device based on $MnFe_2O_4$/graphene hybrids with mass loading of 0.4 mg was also recorded. Furthermore, Energy-dispersive X-ray spectrometry (EDS) mapping analysis of elements Fe, Mn, C, and O (Fig. 2F) confirms the well-distribution of $MnFe_2O_4$ microspheres on graphene sheets. Besides, the EDS spectra of the as-prepared $MnFe_2O_4$/graphene hybrids (Fig. 3A) confirm the presence of C, Mn, Fe, O.

To further verify the composition of the prepared products, X-ray photoelectron spectroscopy (XPS) analysis was applied to investigate both the concentration and binding energy of surface atoms present in the as-synthesized $MnFe_2O_4$/graphene hybrids. In the survey spectrum (Fig. 3B), the elements Mn, Fe, C, and O could be observed. The binding energy values of Fe2p and Mn2p for the sample were found to be 708.7 and 638.8 eV, respectively. The obtained results obviously confirm that both iron ions and manganese ions are present in $MnFe_2O_4$/graphene hybrids. Besides, the atomic concentrations of Fe2p and Mn2p in the hybrids are 2.2% and 1.4%, respectively, which reveals the molar ratio of Mn/Fe close to 1:2. We could see from Fig. 3C that high resolution XPS spectrum of Mn2p shows that Mn is in the +2 oxidation state in the hybrids.

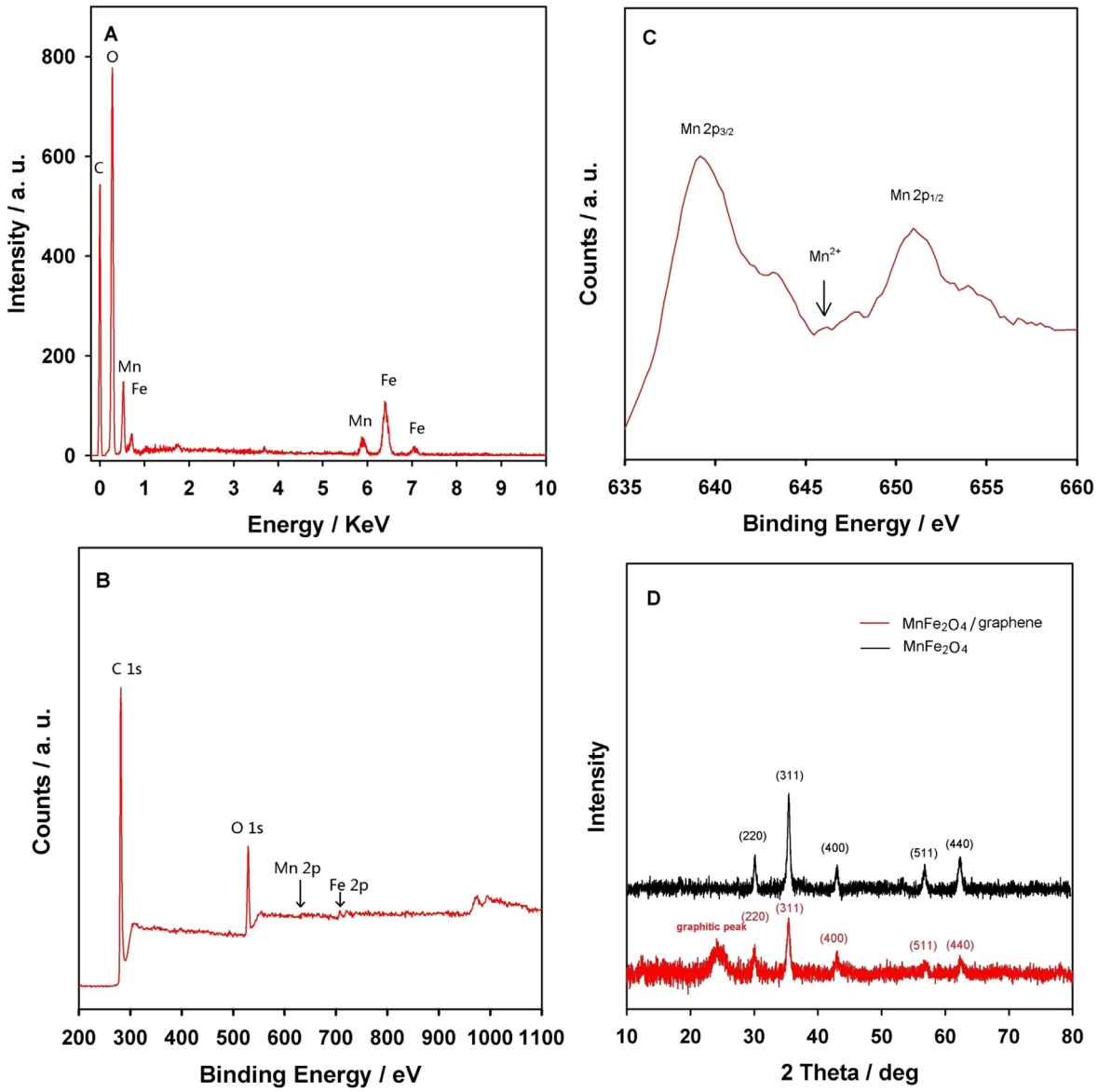

Fig. 3. (A) EDS of $MnFe_2O_4$/graphene hybrids; (B) wide and deconvoluted (C) XPS spectra of the as-prepared $MnFe_2O_4$/graphene hybrids; (D) XRD pattern of $MnFe_2O_4$ (black curve) and $MnFe_2O_4$/graphene hybrids (red curve). (For interpretation of the references to color in this figure legend, the reader is referred to the web version of this article.)

The binding energy of Mn2p3/2 and Mn2p1/2 are 639.2 and 651.1 eV, which is in conformity with the results reported [28].

To obtain sufficient crystal phase of $MnFe_2O_4$ and $MnFe_2O_4$/graphene, both the $MnFe_2O_4$ (black curve) and $MnFe_2O_4$/graphene (red curve) were characterized by X-ray diffraction (XRD) (Fig. 3D). The diffraction peaks correspond to the (220), (311), (400), (511), and (440) crystal planes of cubic spinel structural $MnFe_2O_4$ (JCPDS 74-2403) [25]. A broad peak appeared at $2\theta = 24.16^\circ$ in the XRD pattern of $MnFe_2O_4$/graphene is associated to two different lattice spacing between basal planes of graphene sheets [29].

The three-electrode system was applied for electrochemical measurements and 1.0 M H_2SO_4 aqueous solution was used as electrolyte. s-Graphene and $MnFe_2O_4$ modified electrodes were also tested as comparisons, as shown in Fig. 4A. It is obviously seen that GTS itself attributes no electrochemical capacitance. However, the $MnFe_2O_4$/graphene modified electrode exhibits profound reversible redox peaks with largest capacitance among the four electrodes. To evaluate the contribution of $MnFe_2O_4$ to the capacitance of the $MnFe_2O_4$/graphene hybrids modified electrodes, we carried out a detailed study of the impact of the ferrite's loading on the capacitance. First, the galvanostatic charge/discharging curves (CC curves, Fig. 4B and C) of different modified electrodes were recorded at a current density of 0.3 A g^{-1}. As shown in Fig. 4D, with the increase of the loading of $MnFe_2O_4$, the capacitance decreases obviously. Furthermore, the pure $MnFe_2O_4$ modified electrode only achieves a capacitance of 8 F g^{-1}. The poor capacitance of $MnFe_2O_4$ may result from its low electrical conductivity (1.64 S m^{-1} for $MnFe_2O_4$ modified GTS electrodes and 1.44×10^4 S m^{-1} for GTS electrodes, Fig. S2A–C). Though we could see that s-graphene without $MnFe_2O_4$ possesses a capacitance of 89 F g^{-1}, $MnFe_2O_4$/graphene exhibits a high capacitance of 300 F g^{-1} at a current density of 0.3 A g^{-1}. The severe agglomeration of s-graphene probably leads to limited capacitance of s-graphene. Fortunately, graphene sheets which can provide highways for the transport of electrons were adopted to anchor $MnFe_2O_4$ microspheres. Meanwhile, $MnFe_2O_4$ can also act as separating agents to prevent graphene layers from restacking [16]. Detailed studies were carried out to further explore the impact of the mass loading (0.2–0.5 mg cm^{-2}) of the hybrids. As shown in

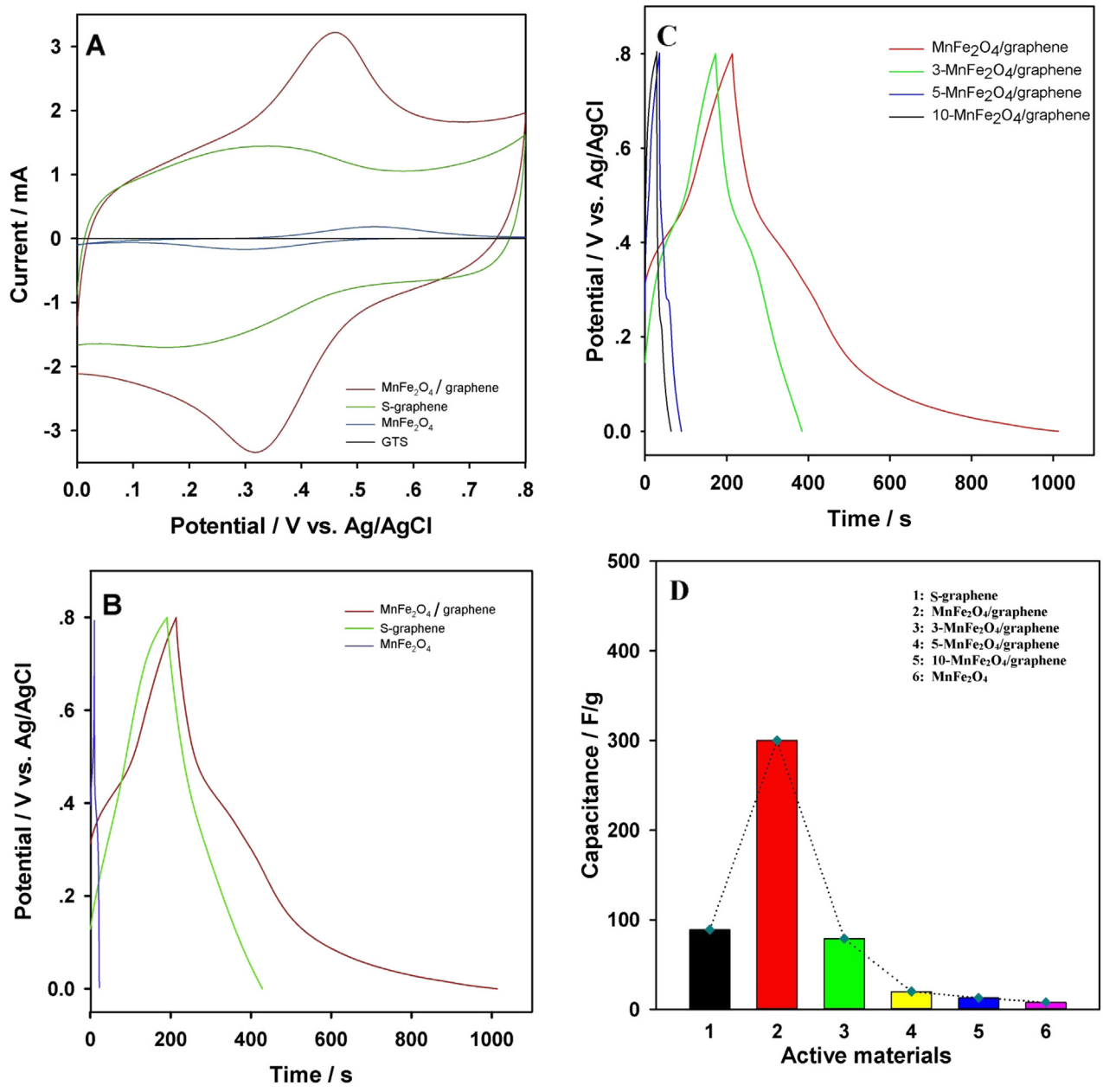

Fig. 4. (A) CV curves of GTS, s-graphene, $MnFe_2O_4$, $MnFe_2O_4$/graphene hybrids obtained at a scan rate of 100 mV s^{-1} in 1.0 M H_2SO_4 solution; (B) CC curves of s-graphene, $MnFe_2O_4$, $MnFe_2O_4$/graphene hybrids at a current density of 0.3 A g^{-1}; (C) CC curves of $MnFe_2O_4$, 3-$MnFe_2O_4$/graphene, 5-$MnFe_2O_4$/graphene, 10-$MnFe_2O_4$/graphene at a current density of 0.3 A g^{-1}; (D) the specific capacitances based on different active materials.

Fig. S3A, cyclic voltammogram (CV) shows that the current response increases with the increase of the mass loading of $MnFe_2O_4$/graphene. But an optimal mass loading (0.2 mg cm^{-2}) could be found while galvanostatic charge/discharging measurements (Fig. S3B) were performed at a current density of 0.3 A g^{-1}. So a mass loading value of 0.2 mg cm^{-2} was chosen in the following measurements.

The two-electrode system was also used to test the assembled supercapacitors to explore the advantages of these flexible electrochemical capacitors for real applications. Fig. 5A displays the CV curves of three supercapacitors which are based on $MnFe_2O_4$ (green curve in web version), s-graphene (red curve in web version) and $MnFe_2O_4$/graphene (black curve), respectively. As seen from Fig. 5A, the current densities of $MnFe_2O_4$/graphene are nearly two times higher than that of the s-graphene and are two orders of magnitude larger than that of $MnFe_2O_4$. The rectangular shapes and symmetry of the CV scans indicate its ideal pseudocapacitive nature, from the scan rates of 10–1000 mV s^{-1} (Fig. 5B). CC curves (Fig. 5C, D) at various current densities were also recorded to further evaluate the performance of the flexible device based on $MnFe_2O_4$/graphene. These charge curves are relatively symmetric to their corresponding discharge counterparts at the current densities from 0.5 to 2.5 A g^{-1}, further revealing the good capacitive behavior of the flexible all-solid-state supercapacitors. It can be seen that an all-solid-state supercapacitor based on $MnFe_2O_4$/graphene hybrids could achieve a high gravimetric specific capacitance of 120 F g^{-1} at 0.1 A g^{-1} and 113 F g^{-1} even at high current density of 1 A g^{-1} (Fig. 5E, data calculated from Fig. 5C, D).

Interestingly, unlike the MnO_2 based on supercapacitors, the supercapacitors based on $MnFe_2O_4$/graphene retain about 105% of the initial capacitance after 5000 cycles (Fig. 5F). $MnFe_2O_4$/

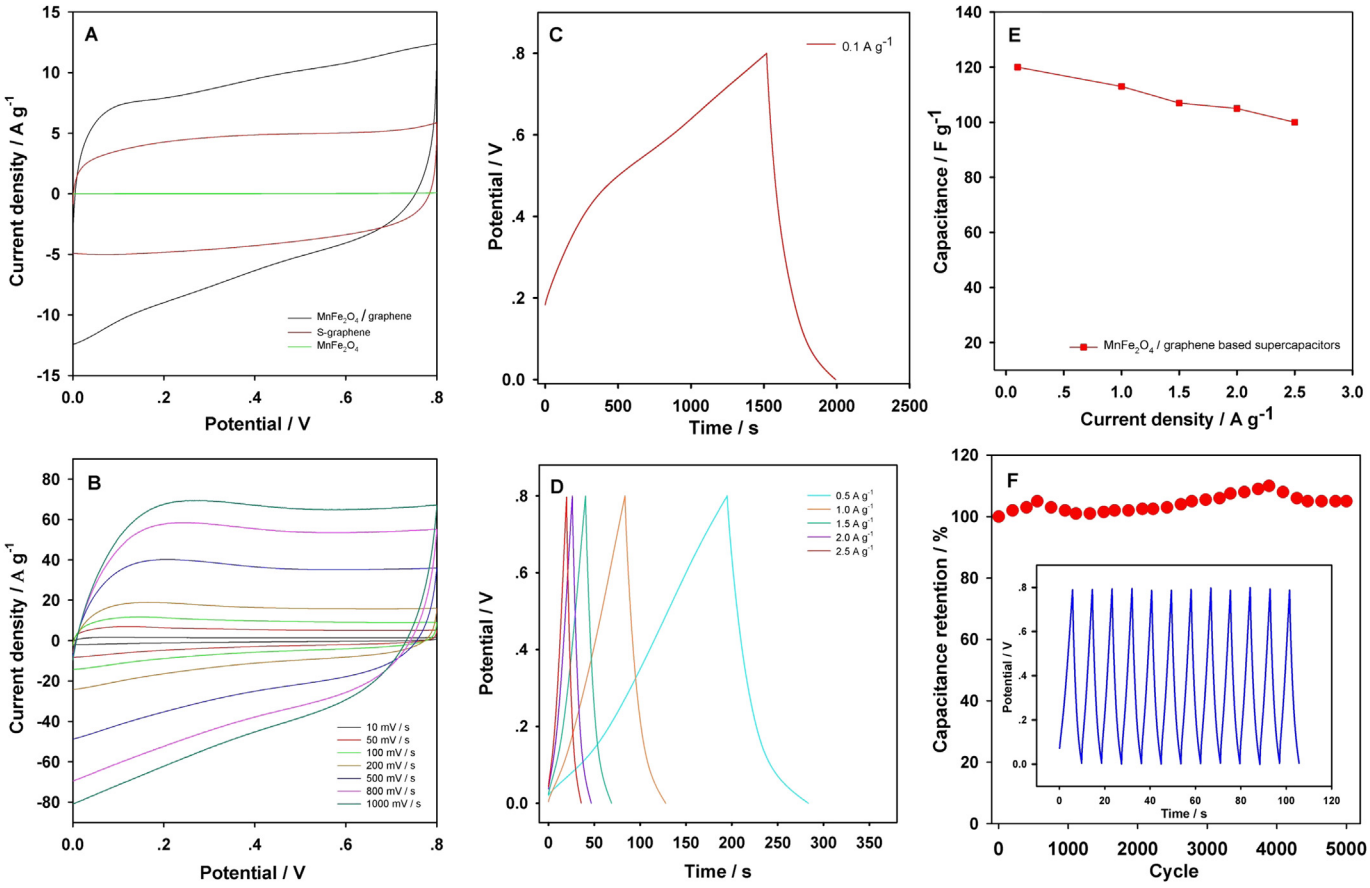

Fig. 5. (A) CV curves for supercapacitors based on s-graphene, $MnFe_2O_4$, and $MnFe_2O_4$/graphene hybrids; (B) CV curves for a supercapcitor based on $MnFe_2O_4$/graphene hybrids at various scan rates, from 10 to 1000 mV s^{-1}; (C) CC curve for a supercapcitor based on $MnFe_2O_4$/graphene hybrids at 0.1 A g^{-1}; (D) CC curves for a supercapcitor based on $MnFe_2O_4$/graphene hybrids at different current densities from 0.5 to 2.5 A g^{-1}; (E) the gravimetric specific capacitances of a supercapacitor based on $MnFe_2O_4$/graphene hybrids at different current densities; (F) cycling stability of a supercapacitor based on $MnFe_2O_4$/graphene hybrids over 5000 cycles at a current density of 5 A g^{-1}, with the CC curves of the corresponding supercapacitors in the inset.

graphene hybrids based supercapacitors show excellent long-term cycling stability probably partially because of the spinel type structure of $MnFe_2O_4$. The excellent long-term cycling stability of our supercapacitors based on 10-$MnFe_2O_4$/graphene hybrids (Fig. S4) further confirms that the addiction of $MnFe_2O_4$ could not affect the cycling stability of our supercapacitors though we know graphene could also help to improve the cycling stability. These results indicate our supercapacitors have promising perspectives in the real applications. The inset of Fig. 5F shows the corresponding supercapacitor was charged and discharged for 12 cycles at a current density of 5 A g^{-1}.

Electrochemical impedance spectroscopy (EIS) confirms the fast ion transport within the $MnFe_2O_4$/graphene electrodes. EIS measurements were conducted among $MnFe_2O_4$, s-graphene and $MnFe_2O_4$/graphene based supercapacitors in the frequency range 0.1 Hz–100 kHz at open-circuit voltage. As shown in Fig. 6, the data could be nicely fit with the equivalent circuit (in the inset of Fig. 6). The R_e values for s-graphene (2.1 Ω), $MnFe_2O_4$/graphene (3.5 Ω) and $MnFe_2O_4$ (4.0 Ω) are quite approximately the same, which means that the electrodes obtained by different materials have the similar combination resistance of electrolyte and contact resistance at the active material/current collector interface. Moreover, the semicircle portion at high frequencies corresponds to the charge transfer limiting process and the charge transfer resistance (R_{ct}) refers to the semicircle diameter. A semicircle of about 80 kΩ in diameter for $MnFe_2O_4$ (black bubbles) indicates a poor electron transfer process.

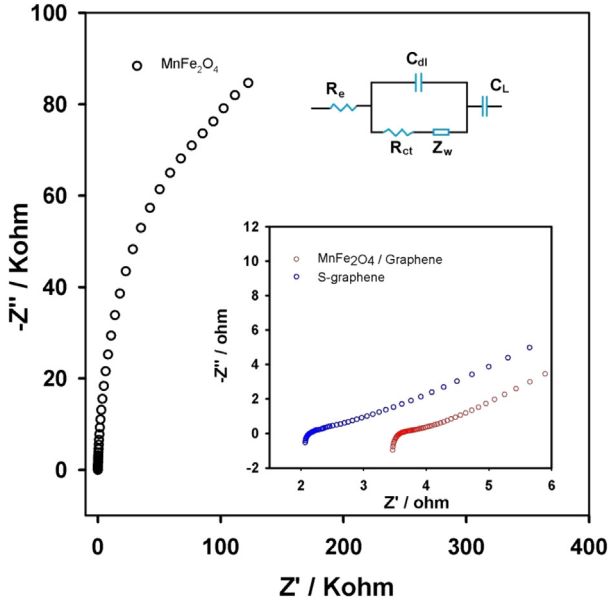

Fig. 6. Complex plane plot of the impedance of $MnFe_2O_4$ based supercapacitors (black bubbles), with an equivalent circuit model, the plots of s-graphene (blue bubbles) based supercapacitors and $MnFe_2O_4$/graphene hybrids based supercapacitors (red bubbles) in the inset. (For interpretation of the references to color in this figure legend, the reader is referred to the web version of this article.)

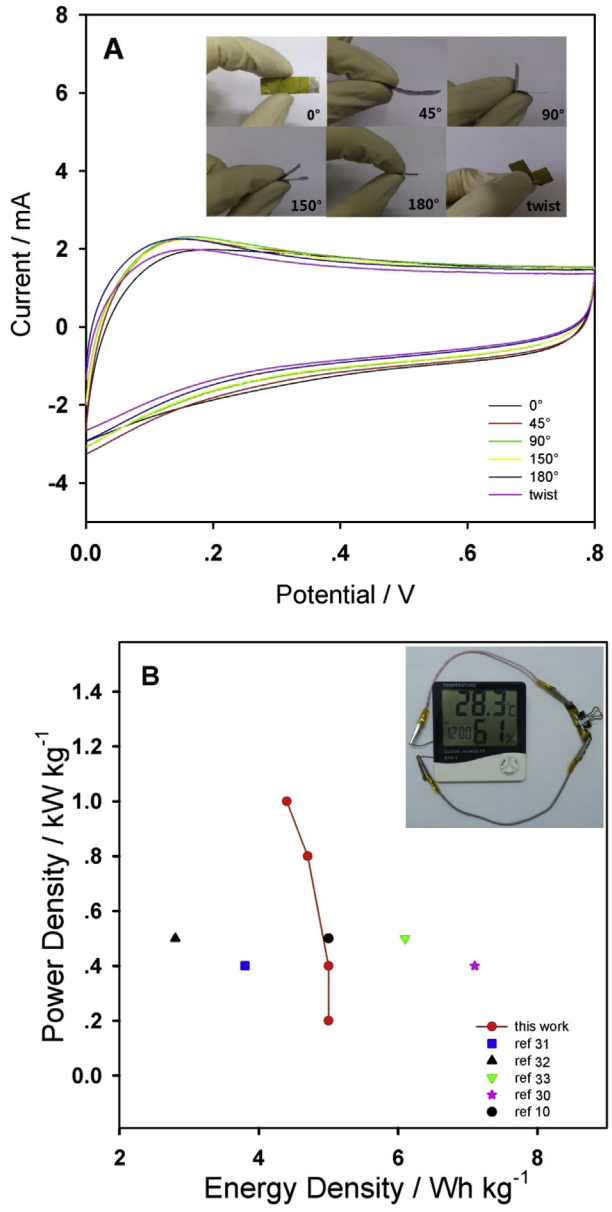

Fig. 7. (A) CV curves for a supercapacitor based on $MnFe_2O_4$/graphene hybrids at different curvatures of 0°, 45°, 90°, 150°, 180° and in twisted condition, with the corresponding digital images in the inset; (B) Ragone plots (power density *vs* energy density) comparing the $MnFe_2O_4$/graphene based supercapacitors to previously reported solid-state devices, with a digital photograph of LCD driven by two devices in series in the inset.

However, the R_{ct} value for $MnFe_2O_4$/graphene hybrids decreases to only 1.0 Ω, after $MnFe_2O_4$ was grown on graphene nanosheets. This dramatical decrease mainly benefits from the excellent conductivity of s-graphene (R_{ct} value of only 0.5 Ω). The series resistance of the $MnFe_2O_4$/graphene based device is estimated to be 4.5 Ω which is much lower than that of a laser scribing based supercapacitor (16 Ω) [30]. From the above analysis, it can be concluded that $MnFe_2O_4$/graphene hybrids have a superior capacitive performance, which is in consistent with the other electrochemical tests conducted above.

Our flexible all-solid-state supercapacitors also show excellent mechanical robustness in the bending and twisting test. The CV performance of this device under different conditions is shown in Fig. 7A (Insets are the corresponding digital images at various bending angles and in twisted condition). There are no significant differences as the bending angles changed from 0° to 180° or in twisted condition, demonstrating that the changes of electrochemical property are negligible under different bending angles or in twisted condition.

Fig. 7B displays Ragone plots (power density *vs* energy density) to compare our devices with previously reported solid-state supercapacitors [30–33]. Note that, the power density and energy density shown in the inset of Fig. 5D are based on the active materials. It can be seen that our flexible supercapacitors exhibit a power density (0.4 kW kg^{-1}) and energy density (5.0 Wh kg^{-1}) that are comparable to flexible supercapacitors based on three-dimensional graphene/MnO_2 composite networks (0.5 kW kg^{-1} and 5.0 Wh kg^{-1}) [10]. To verify the potential usefulness of this facile approach to fabricate $MnFe_2O_4$/graphene hybrids based flexible all-solid-state supercapacitors, we have connected two supercapacitors units in series to make a tandem device. It was found that the tandem device could successfully drive a liquid crystal display (1.5 V LCD, inset of Fig. 7B), revealing the practical potential of the flexible supercapacitors.

4. Conclusion

We have reported a facile approach to fabricate all-solid-state supercapacitors based on $MnFe_2O_4$/graphene hybrids to achieve a high gravimetric specific capacitance (120 F g^{-1} at 0.1 A g^{-1}), excellent cycling stability (retaining 105% capacitance after 5000 cycles) and outstanding mechanical flexibility. These findings demonstrate that our proposed approach may have promising potential in the preparation of flexible supercapacitors based on other active materials which are in powders condition at first.

Acknowledgment

The authors gratefully acknowledge the financial support by NSFC (21372088).

Appendix A. Supplementary data

Supplementary data related to this article can be found at http://dx.doi.org/10.1016/j.jpowsour.2014.01.027.

References

[1] Y. He, W. Chen, C. Gao, J. Zhou, X. Li, E. Xie, Nanoscale 5 (2013) 8799–8820.
[2] C. Huang, P.S. Grant, Sci. Rep. 3 (2013) 2393.
[3] H.Y. Jung, M.B. Karimi, M.G. Hahm, P.M. Ajayan, Y.J. Jung, Sci. Rep. 2 (2012) 773.
[4] J.H. Park, J.M. Ko, O.O. Park, J. Electrochem. Soc. 150 (2003) A864–A867.
[5] W. Sugimoto, T. Kizaki, K. Yokoshima, Y. Murakami, Y. Takasu, Electrochim. Acta 49 (2004) 313–320.
[6] B.J. Lee, S.R. Sivakkumar, J.M. Ko, J.H. Kim, S.M. Jo, D.Y. Kim, J. Power Sources 168 (2007) 546–552.
[7] X. Zhang, W. Shi, J. Zhu, D.J. Kharistal, W. Zhao, B.S. Lalia, H.H. Hng, Q. Yan, ACS Nano 5 (2011) 2013–2019.
[8] D.P. Dubal, G.S. Gund, R. Holze, H.S. Jadhav, C.D. Lokhande, C.-J. Park, Dalton Trans. 42 (2013) 6459–6467.
[9] D.P. Dubal, G.S. Gund, R. Holze, C.D. Lokhande, J. Power Sources 242 (2013) 687–698.
[10] Y. He, W. Chen, X. Li, Z. Zhang, J. Fu, C. Zhao, E. Xie, ACS Nano 7 (2013) 174–182.
[11] L. Peng, X. Peng, B. Liu, C. Wu, Y. Xie, G. Yu, Nano Lett. 13 (2013) 2151–2157.
[12] S. Santhanagopalan, A. Balram, D.D. Meng, ACS Nano 7 (2013) 2114–2125.
[13] C. Yuan, L. Yang, L. Hou, J. Li, Y. Sun, X. Zhang, L. Shen, X. Lu, S. Xiong, X.W. Lou, Adv. Funct. Mater. 22 (2012) 2560–2566.
[14] C.-W. Kung, H.-W. Chen, C.-Y. Lin, R. Vittal, K.-C. Ho, J. Power Sources 214 (2012) 91–99.
[15] J. Xu, Q. Wang, X. Wang, Q. Xiang, B. Hang, D. Chen, G. Shen, ACS Nano 7 (2013) 5453–5462.
[16] S.D. Perera, A.D. Liyanage, N. Nijem, J.P. Ferraris, Y.J. Chabal, K.J. Balkus Jr., J. Power Sources 230 (2013) 130–137.

[17] Z. Chen, V. Augustyn, J. Wen, Y. Zhang, M. Shen, B. Dunn, Y. Lu, Adv. Mater. 23 (2011) 791–795.
[18] J.S. Bonso, A. Rahy, S.D. Perera, N. Nour, O. Seitz, Y.J. Chabal, K.J. Balkus Jr., J.P. Ferraris, D.J. Yang, J. Power Sources 203 (2012) 227–232.
[19] Q. Qu, Y. Zhu, X. Gao, Y. Wu, Adv. Energy Mater. 2 (2012) 950–955.
[20] M. Yu, T. Zhai, X. Lu, X. Chen, S. Xie, W. Li, C. Liang, W. Zhao, L. Zhang, Y. Tong, J. Power Sources 239 (2013) 64–71.
[21] S.L. Kuo, N.L. Wu, Electrochem. Solid State Lett. 8 (2005) A495–A499.
[22] S.-L. Kuo, N.-L. Wu, J. Power Sources 162 (2006) 1437–1443.
[23] M. Sathish, T. Tomai, I. Honma, J. Power Sources 217 (2012) 85–91.
[24] N.I. Kovtyukhova, P.J. Ollivier, B.R. Martin, T.E. Mallouk, S.A. Chizhik, E.V. Buzaneva, A.D. Gorchinskiy, Chem. Mater. 11 (1999) 771–778.
[25] S. Bai, X. Shen, X. Zhong, Y. Liu, G. Zhu, X. Xu, K. Chen, Carbon 50 (2012) 2337–2346.
[26] C. Nethravathi, M. Rajamathi, Carbon 46 (2008) 1994–1998.
[27] H. Deng, X.L. Li, Q. Peng, X. Wang, J.P. Chen, Y.D. Li, Angew. Chem. Int. Ed. 44 (2005) 2782–2785.
[28] S. Matzen, J.B. Moussy, R. Mattana, K. Bouzehouane, C. Deranlot, F. Petroff, J.C. Cezar, M.A. Arrio, P. Sainctavit, C. Gatel, B. Warot-Fonrose, Y. Zheng, Phys. Rev. B 83 (2011) 184402.
[29] V. Strong, S. Dubin, M.F. El-Kady, A. Lech, Y. Wang, B.H. Weiller, R.B. Kaner, ACS Nano 6 (2012) 1395–1403.
[30] M.F. EI-Kady, V. Strong, S. Dubin, R.B. Kaner, Science 335 (2012) 1326–1330.
[31] M. Kaempgen, C.K. Chan, J. Ma, Y. Cui, G. Gruner, Nano Lett. 9 (2009) 1872–1876.
[32] Y.J. Kang, H. Chung, C.-H. Han, W. Kim, Nanotechnology 23 (2012) 065401.
[33] Y. Xu, Z. Lin, X. Huang, Y. Liu, Y. Huang, X. Duan, ACS Nano 7 (2013) 4042–4049.